

A Review of Aeronautical Fatigue Investigations in Sweden During the Period April 2013 to March 2015



Edited by HANS ANSELL
Saab AB
Sweden

ICAF Doc. No. 2431
Saab Doc. No. LN-023315



SAAB



FOI



Linköping University



SIEMENS

Presented at the 34th Conference of the International Committee on Aeronautical Fatigue and Structural Integrity (ICAF), Helsinki, Finland, 1-2 June 2015.

CONTENT

1. INTRODUCTION
2. STRUCTURAL INTEGRITY CHARACTERISTICS OF METAL MATERIALS AND STRUCTURE
 - 2.1. Comparable crack growth tests with 7050-T7451 and aluminum-lithium AA2050-T84 alloys in thick plate form
 - 2.2. Fatigue testing of the Cr(VI)- free surface treatments TSA and PAA on thick aluminium plates
 - 2.3. Stress Analyses and Stress Intensities for Part-Through Cracks in Bolted Joints Exhibiting Secondary Bending
 - 2.4. Fatigue, none destructive testing (NDT) and design limitation Investigations for additive manufactured (AM, 3d-printing) metallic materials
3. STRUCTURAL INTEGRITY CHARACTERISTICS OF COMPOSITE MATERIALS AND STRUCTURE
 - 3.1. Bearing Failure of CFRP Composite in Biaxially Loaded Bolted Joints at Elevated Temperature
 - 3.2. Numerical and experimental study of buckling and collapse of hybrid and integral composite panels – POSCOS
 - 3.3. Development and implementation of a method for in-service interpretation and decision regarding temporary acceptance of damage in composite structure
 - 3.4. Analysis and testing of a linerless demonstrator tube at cryogenic temperatures and made of thin carbon plies
4. THERMAL MECHANICAL FATIGUE CHARACTERISTICS OF SUPERALLOYS
 - 4.1. Dwell time crack growth at high temperature in a Ni-based superalloy
 - 4.2. Test facility for Thermal Mechanical Fatigue – TMF
 - 4.3. Mechanical behaviour and microstructure in selective laser melted Hastelloy X

ACKNOWLEDGEMENTS

1 INTRODUCTION

In this paper a review is given of the work carried out in Sweden in the area of aeronautical fatigue and structural integrity during the period April 2013 to March 2015. The review includes basic studies and industrial applications. The review is brief for the current period mainly because of the very extensive development work that has taken place on the Gripen NG aircraft. This engagement has consumed resources that otherwise would have been devoted to general research and development of interest for the aeronautical community.

Contributions to the present review are from the following bodies:

- Saab AB
Sections 2.1, 2.2, 2.3, 2.4, 3.1, 3.2, 3.3
- The Swedish Defence Research Agency (FOI)
Sections 3.1, 3.2, 3.4
- Linköping University (LiU)
Sections 4.1
- Exova Technology AB
Sections 4.2
- Siemens Turbomachinery AB
Sections 4.3

2 FATIGUE AND DAMAGE TOLERANCE CHARACTERISTICS OF METAL MATERIAL AND STRUCTURE

2.1 Comparable crack growth tests with 7050-T7451 and aluminum-lithium AA2050-T84 alloys in thick plate form.

Hans Ansell, Zlatan Kapidžić, Saab AB

It is known that dislocation glide occurs within grains predominately along a single slip system in alloys in the under-aged condition which promotes a serrated crack path. Aluminium-Lithium alloy AA2050-T84 is in such an under-aged condition. Spectrum tests on conventional specimen (CCT, CT) for obtaining design data for the alloy showed in some cases results of this kind which needed further investigation by additional testing. The main interest was to investigate the crack behavior in geometries which is more airframe-like than specimens commonly used for material property determination.

1. Surface crack in a notch (Specimen type R)
2. Corner crack open hole (Specimen type H)
3. Corner crack at a pin loaded hole (Specimen type P)

Comparative tests with alloy AA7050-T7451, i.e. in an over-aged condition, were also done.

A test program including the three types of test specimens and associated part-through cracks was conducted. All test specimens were provided with initial defects. The defects were produced by electro-spark machining. The bottom radius was typically 0.030 mm. A total of 33 specimens were included in the experimental study.

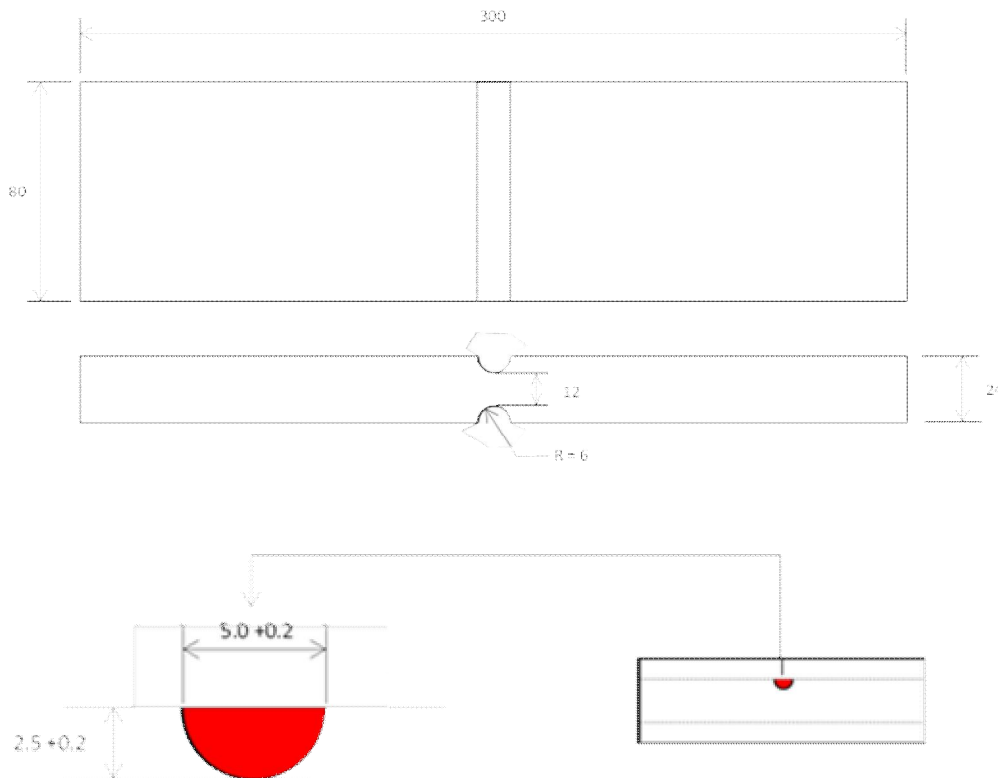


Figure 1. Specimen type R with a surface crack in a circular notch

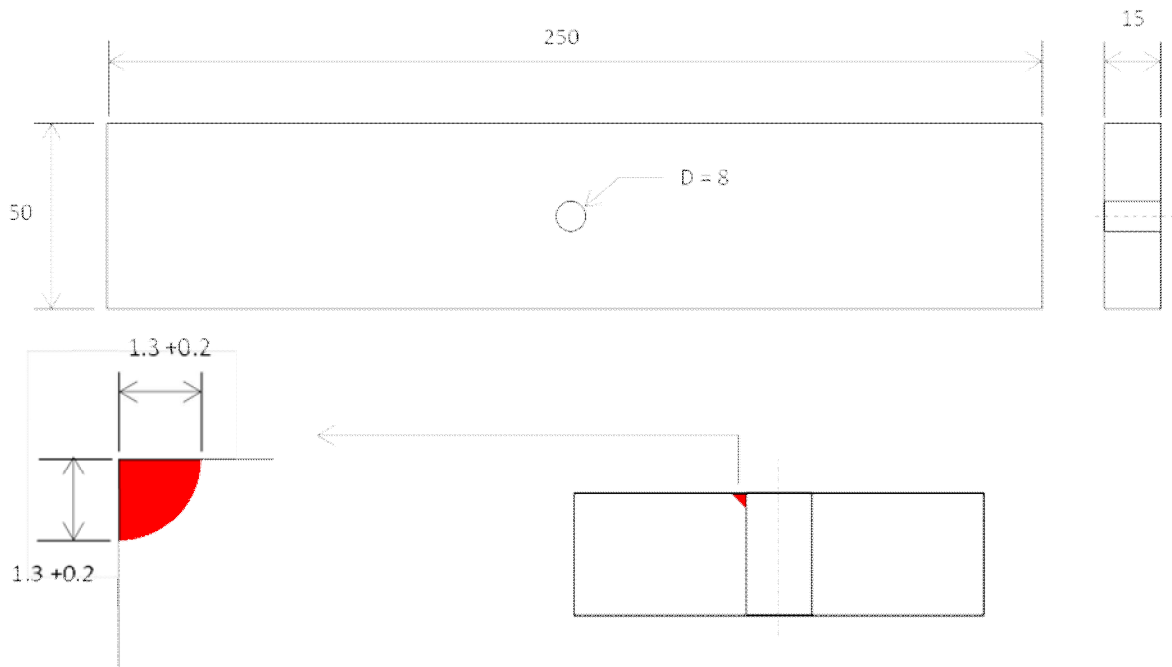


Figure 2. Specimen type H with a corner crack in an open hole

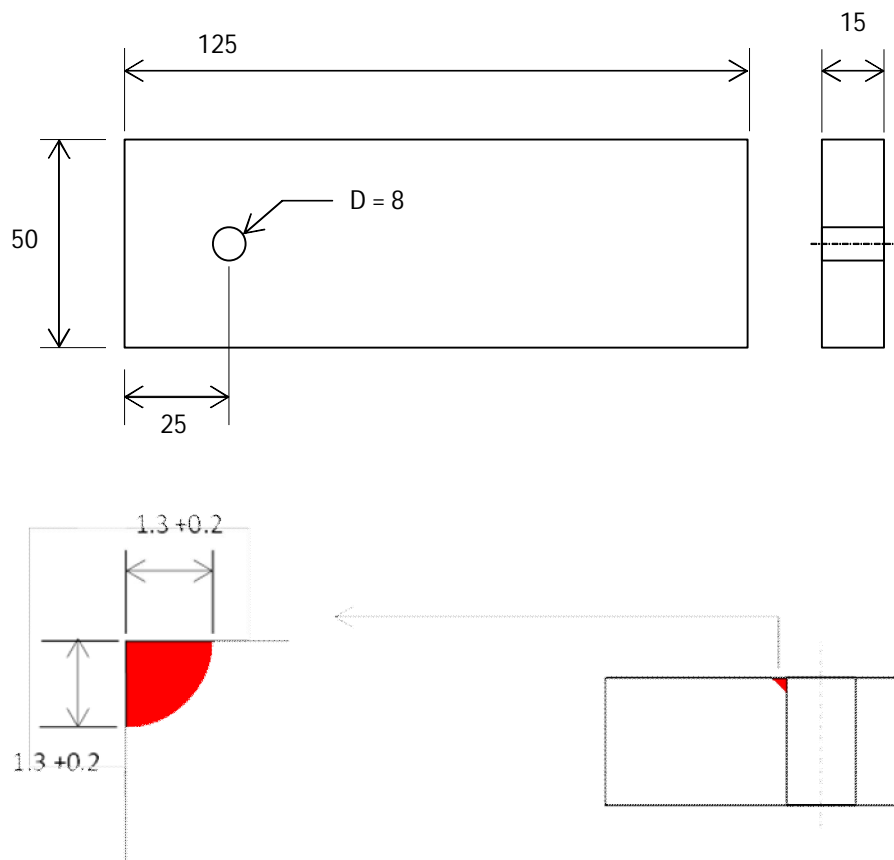


Figure 3. Specimen type P with a corner crack at a pin loaded hole.

The specimens were manufactured from thick plate, 150 mm, with most specimens oriented in the L-S direction (Some P-type specimens in the S-L direction). See figure 4.

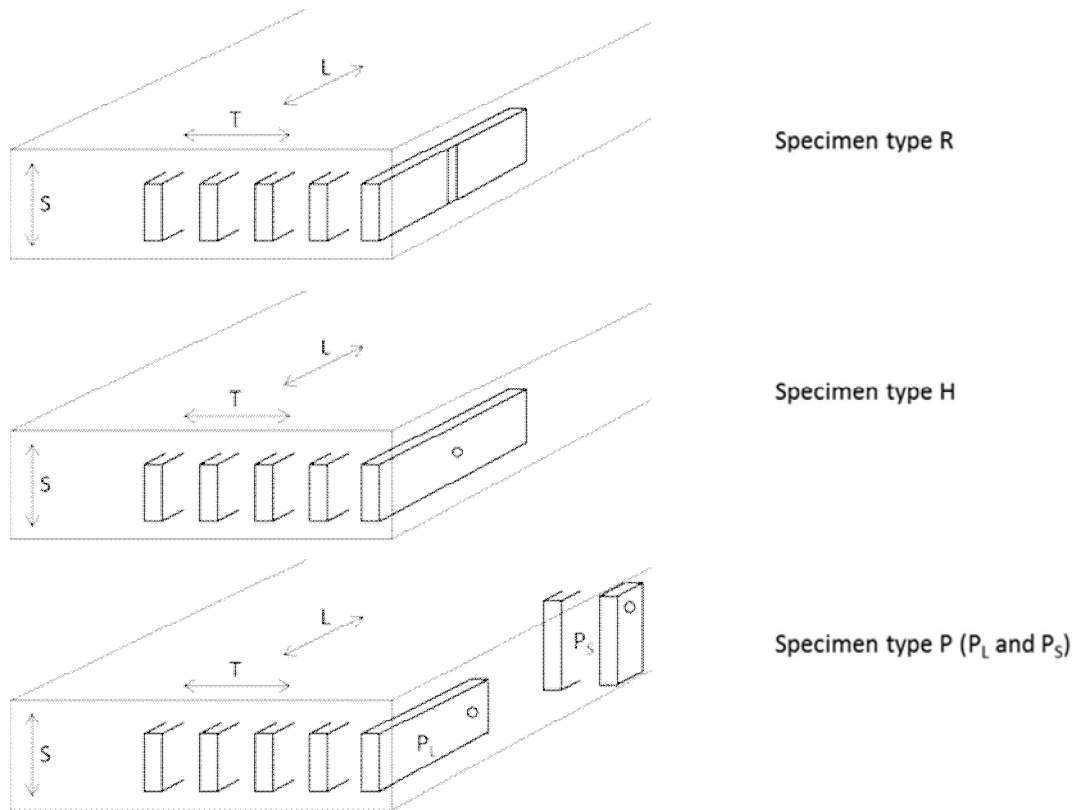


Figure 4. Specimen orientation

Tests were made with both constant amplitude ($R=0.1$ and -1 as reference) and spectrum loading. Two spectra were used, one representing the tension dominated fighter wing loading (W) and the other the symmetric tension/compression fin loading (F). The wing spectra consisted of ~ 30 cycles/hour and the fin spectra ~ 45 cycles/hour. Max spectrum gross stresses were 140 MPa and 120 MPa for W and F type spectra respectively. The tests were stopped before the crack penetrated the "other side" of the test piece in order to quasi-statically load and measure the residual strength when the cracks still were part-through the thickness.

A few results from tests with type R specimens subjected to spectrum type W are shown in figure 5. The test results are shown together with predictions (using constant amplitude data) both with and without using a crack retardations model (no retardation analysis were done for AA2050 alloy due to lack of established model parameters).

It is rather well known that the constant amplitude crack growth rates for AA2050 Al-Li alloy are typically lower than for the more conventional 7050 alloy. This observation seems to remain also under the tension dominated and symmetrical tension-compression type spectra used in this investigation. No particular irregular behavior of the part-through crack surfaces in the 2050 alloy was observed. The crack surfaces looked (on a macroscopic scale) the same in both alloys.

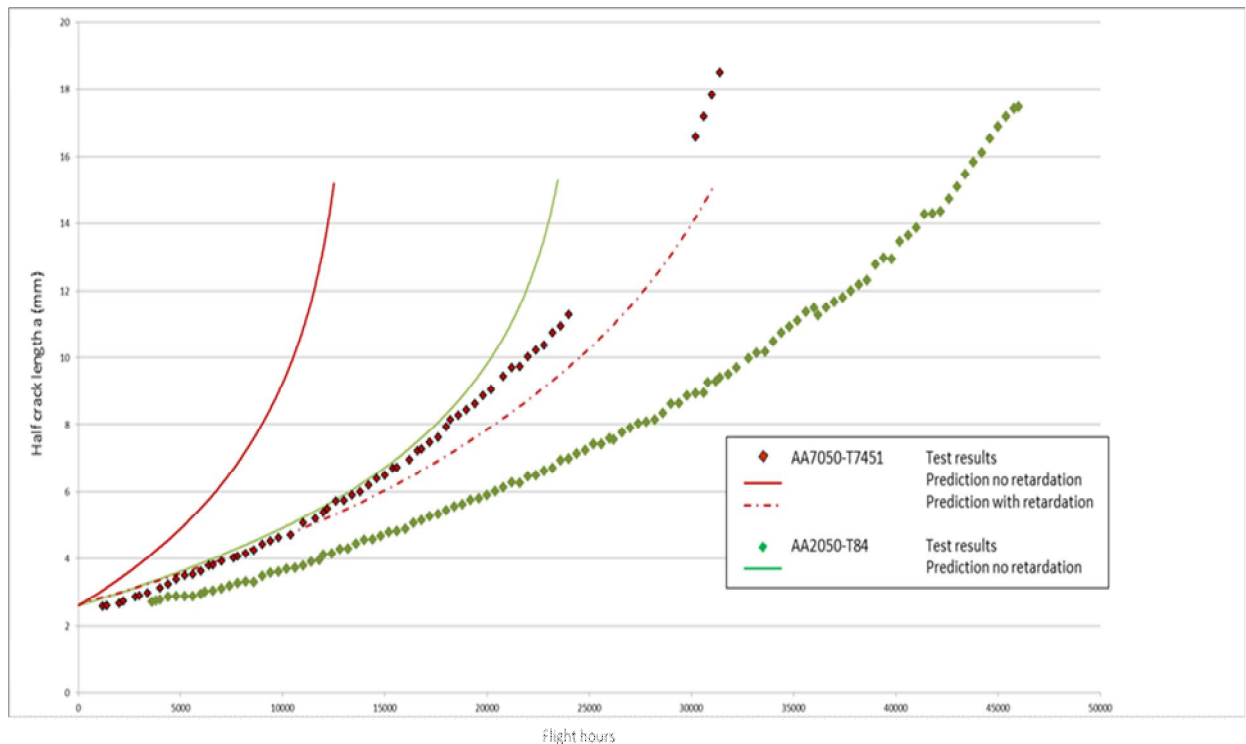


Figure 5. Some test results and comparisons with predictions for specimen type R subjected to spectrum type W.

2.2 Fatigue testing of the Cr(VI)- free surface treatments TSA and PAA on thick aluminium plates

Magnus Kahlin, Saab AB

Environmental regulations in the European Union (REACH) requires that Cr(VI) containing surface treatments are replaced. Two options for Cr(VI)-free anodizing are the TSA, tartaric sulphuric anodizing, and the PAA phosphoric acid anodizing. An extensive fatigue test program to determine the effect of the anodizing processes on fatigue properties on thick aluminium plate 7010 and 2050 has been performed.

Results

The fatigue test results indicate that TSA and PAA anodizing receive similar fatigue behaviour compared to CAA, chromic acid anodizing. The reduction of fatigue strength seems to be controlled by the amount of coarse intermetallic phases (intermetallic compounds), in the aluminium plate surface, which are attacked during the anodizing process. The full surface treatment process, including pickling, anodizing and primer need to be considered when evaluating the effect of surface treatment on fatigue properties.

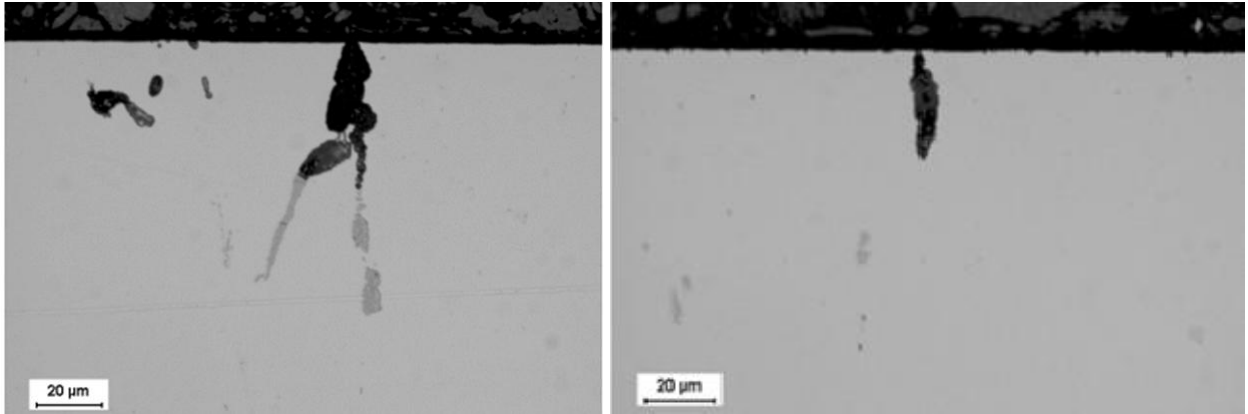


Figure 1. Attacked intermetallic phases in aluminium plates after pickling and anodizing

2.3 Stress Analyses and Stress Intensities for Part-Through Cracks in Bolted Joints Exhibiting Secondary Bending

Zlatan Kapidžić, Hans Ansell and Lars Djärv, Saab AB

The main problems associated with fatigue and damage tolerance in bolted and riveted joints are the crack nucleation and the crack growth at fastener holes. The fatigue and crack growth life are affected by several load parameters: the load transferred through the fasteners, the by-passed load and the secondary bending. The superposition technique to obtain the combined stress intensity factors for cracks at fastener holes is made available in software such as AFGROW, but it requires the proportion of each unit load case to be known. The methods for determining the transferred and the by-passed load are rather well established, while the secondary bending is more difficult to quantify.

In this work [1], the tensile and the bending stress variations along and in the width direction of a shear loaded, bolted single strap joint are studied by detailed finite element analyses, see figure 1. The results are used to estimate the unit load case proportions for crack growth calculations with the superposition technique in AFGROW. Two different joint configurations are considered, one with an aluminium splice plate and one with a steel splice plate, in order to study different amounts of the secondary bending.

The detailed FE-modelling, with extended finite element method (XFEM) and the superposition technique in AFGROW are both used to compute the stress intensity factors for part-through cracks at the outmost fastener holes in the joint members. Constant amplitude crack growth is then calculated by AFGROW and compared to the experimental results. The experimental setup is shown in figure 2.

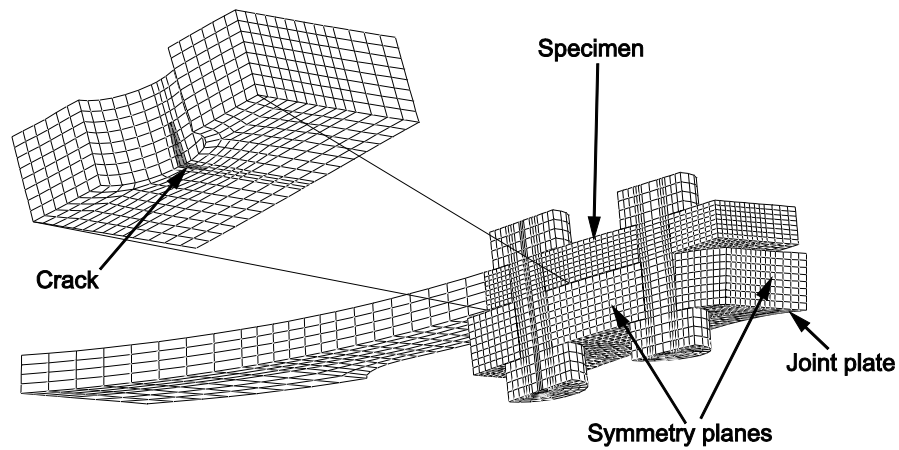


Figure 1. Finite element model of a single strap joint

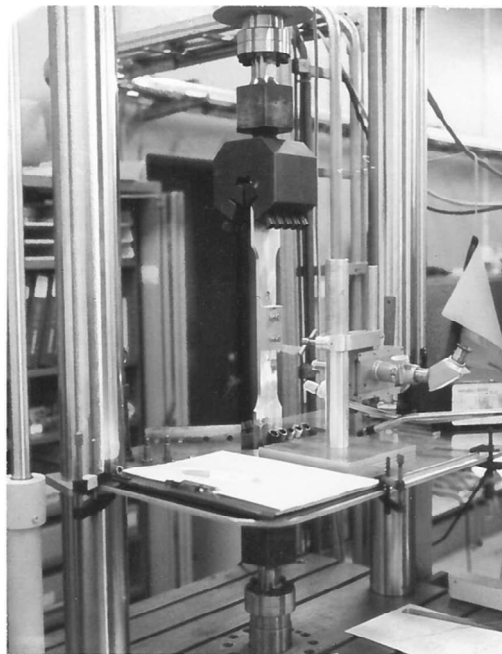


Figure 2. Experimental setup

The analyses show that the bending moment varies along the joint length, with a large gradient in the vicinity of the crack plane, figure 3. The normal stress distribution in the joint crack plane is correctly represented by the axial and bearing unit cases, but the bending stress distribution cannot be represented by the uniform bending unit case. Namely, the bending stress distribution in the joint has a larger stress concentration at the hole than the bending unit case, which is attributed to the tilting of the fastener. Using the bending unit case with the stress determined from the moment at the crack plane in the joint model under predicts the crack growth, while the bending stress determined from the moment in the constant moment area, outside the bolt area, is conservative. Figure 4 shows the comparison between the test results, results based on the XFEM solution and the solution based on the AFGROW unit cases, where the amount of bending is determined by setting the integral of the bending stress in the unit case be equal to the integral of the bending stress in the joint model, over the crack growth distance.

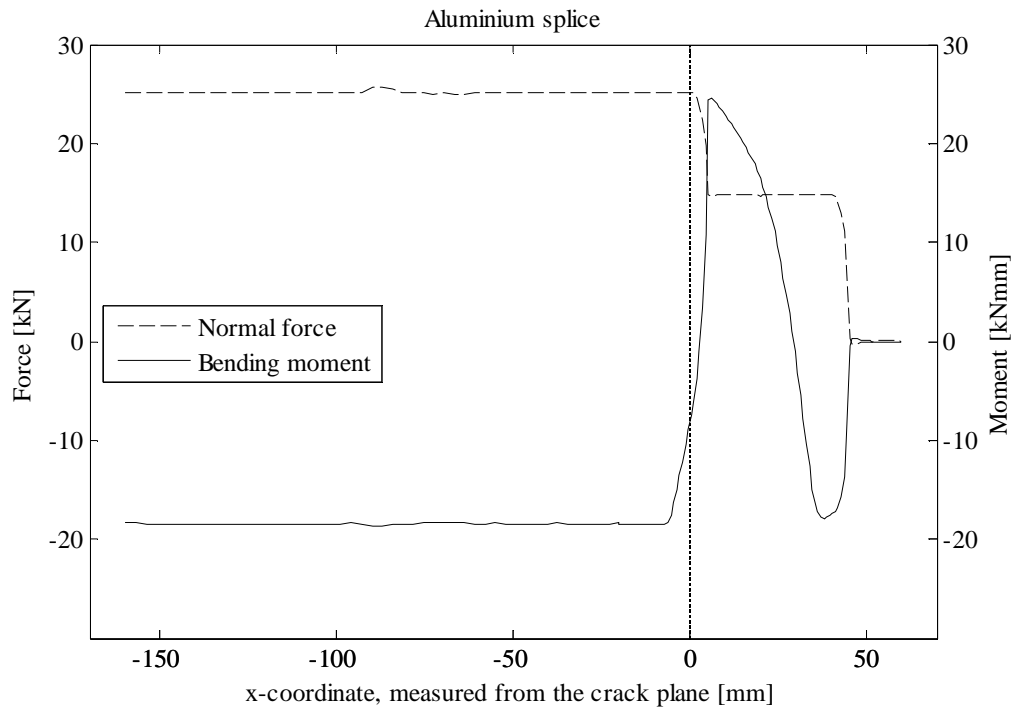


Figure 3. Normal force and bending moment along the joint member

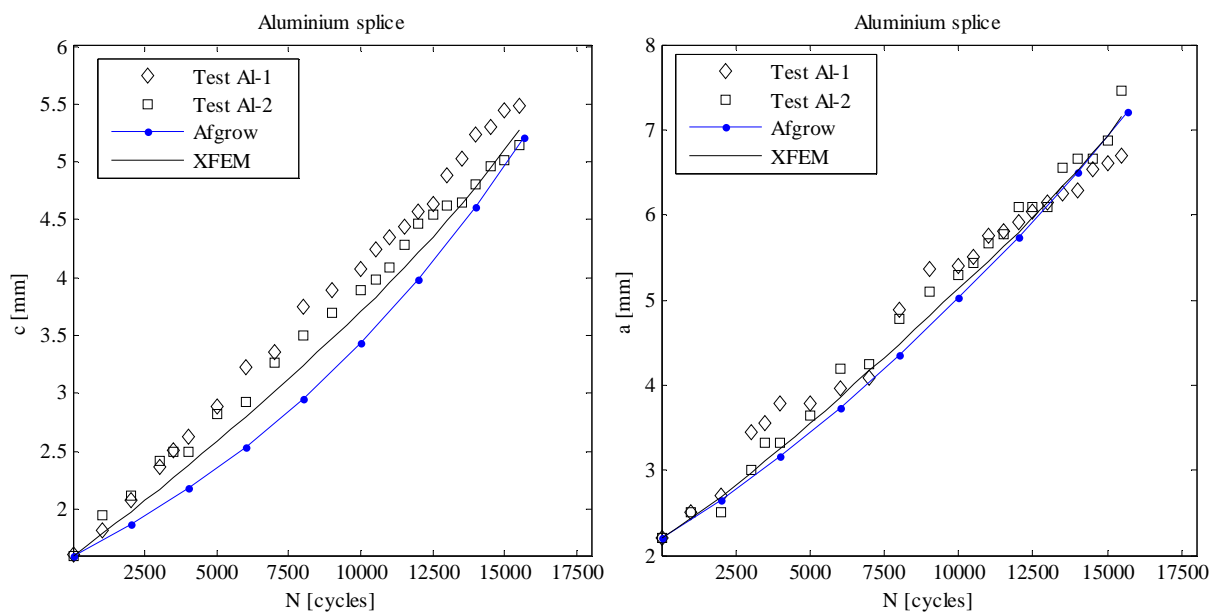


Figure 4. Surface crack length c and through the thickness crack length a , versus the number of cycles N .

- [1] Kapidžić Z, Ansell H, Djärv L. Stress Analyses and Stress Intensities for Part-Through Cracks in Bolted Joints Exhibiting Secondary Bending. 28th ICAF symposium, Helsinki, Finland, 3-5 June 2015

2.4 Fatigue, none destructive testing (NDT) and design limitation investigations for Additive Manufactured (AM, 3d-printing) metallic materials

Magnus Kahlin, Saab AB

Background

Additive manufacturing (AM), 3d-printing, is a relatively new production method that allows the manufacturer to automatically create physical components directly from a computer model. AM can be used to produce industrial parts both lighter in weight, cheaper to produce, and with complex geometries that are difficult or impossible to produce with conventional methods..

The mechanical properties of AM-components however can differ substantially from the properties of the same component produced by conventional techniques. This is due to the complexity of the AM-methods and the large quantity of process parameters. To gain industrial acceptance and be able to introduce AM in high performance applications, a deeper understanding of how the AM process influence fatigue and damage tolerance properties needs to be established as well as verifications of component behavior for AM unique geometries, e.g. lattice or organic structures.

Materials

Titanium AM materials are of primary interest but also aluminium alloys and nickel super alloys are investigated.

Activities

- Investigations of cyclic and static damage tolerances behavior for different AM processes
- Investigations of the fatigue and damage tolerance properties due to variations in process, geometry, build direction and surface roughness
- Establishing limitations for AM design guide lines due to AM material behavior
- Establishing best practices design guide lines for additive manufacturing
- Investigations to determine if conventional methods for FCG simulations can be used for AM material
- Validation of non-destructive testing (NDT) methods for "complex AM geometries"

3 FATIGUE AND DAMAGE TOLERANCE CHARACTERISTICS OF COMPOSITE MATERIALS AND STRUCTURE

3.1 Bearing Failure of CFRP Composite in Biaxially Loaded Bolted Joints at Elevated Temperature

Zlatan Kapidžić, Hans Ansell, Saab AB
Joakim Schön, FOI

Aircraft structures that contain hybrid composite-aluminium joints develop internal loads when exposed to elevated temperatures. The stresses arise due to the different thermal expansion properties of the two material types. In fuselage and wing structures, which contain long rows of fastener installations, the thermally induced load could be oriented in different direction than the applied mechanical load, creating a biaxial bearing load state at the fasteners. Depending on the joint length, the thermally induced bearing load could be of significant magnitude and should then be accounted for. The aim of this study is to characterise and model the static and the fatigue bearing failure of the composite laminate in a hybrid joint and to investigate the influence of the biaxial loading on the fatigue life and static strength. Both experimental methods and numerical analyses are employed.

The experiments were conducted on simple two-bolt, double-lap joints with a carbon fibre reinforced polymer (CFRP) laminate specimens, in uniaxial and biaxial cyclic and static loading at 90 °C. An experimental setup was specifically designed for the purpose, see Fig. 1, where a constant thermally induced bolt load is simulated by means of mechanical load actuators and the mechanical bolt load is applied in the perpendicular direction.

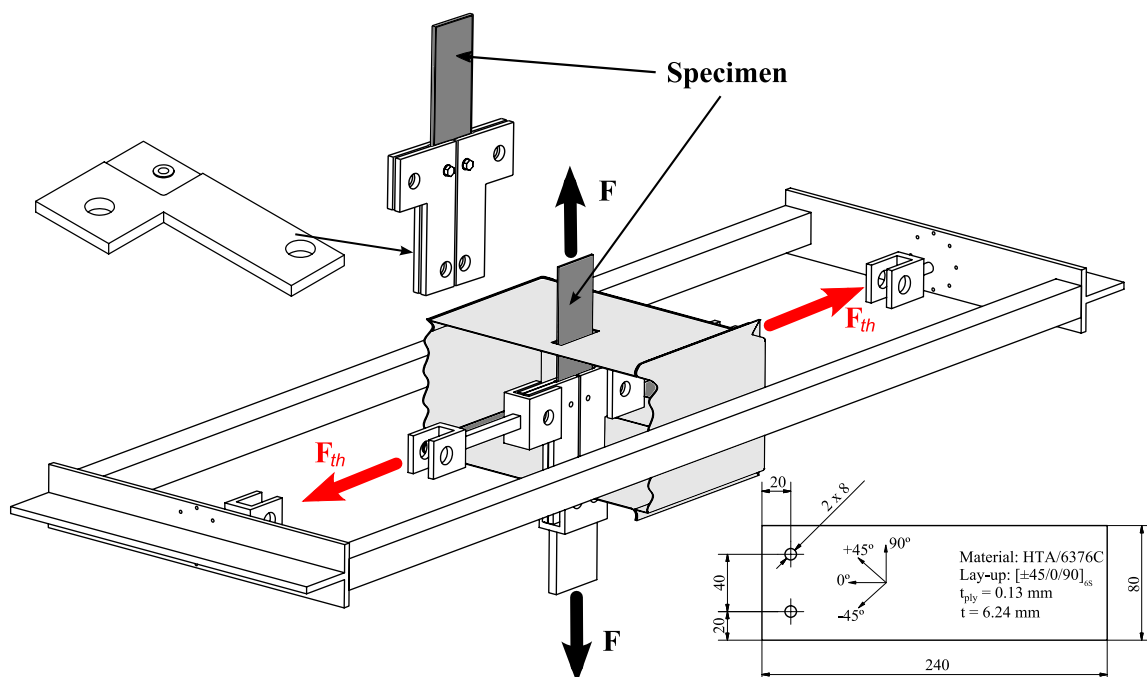


Figure 1. Experimental setup and specimen

The numerical analysis of the joint failure is performed using the finite element method. The static failure model [1] is three-dimensional and includes intralaminar and interlaminar damage progression. Thereby, the matrix and fibre failure within the plies, as well as delamination between the plies is modelled. The fatigue failure model [2] is two-dimensional and is based on the kinetic theory of fracture for polymers. The underlying assumption is that the main driving mechanism of the composite fatigue is matrix cracking. Following this assumption, the multi-continuum theory is employed to obtain the stresses in the matrix which are then passed on as the fatigue driving stresses into the failure criterion. The model describes the appearance of matrix cracks as a thermally activated process promoted by cyclic loading. Consequently, the effects of the temperature, the loading frequency and the load ratio on the crack onset are included in the model.

Figure 2 and 3 show the experimental results compared to the results from the simulations, in terms of the resultant bearing stress, $\sigma_{res}^b = ((F/2)^2 + (F_{th})^2)^{1/2} / (tD)$, where t is the laminate thickness and D is the bolt hole diameter. The static model was able to correctly predict the outcome of the test in terms of the maximum bearing load, the damage initiation load and damage initiation and propagation, in both uniaxial and biaxial loading, see Fig. 2. The simulated damage patterns were compared to results from a microscopy study performed on the bearing plane of the specimens and a good correspondence was observed. The same maximum resultant bearing stress was obtained in the uniaxially and biaxially loaded specimens, although the damage patterns differed between the two. The fatigue prediction model also gave satisfactory results compared to the test results. The model requires a very low material characterization effort and works for fatigue prediction at different temperatures, frequencies and load histories. However, more validation is necessary in order to establish the predictive capability of the model for different geometries, lay-ups, materials, etc. Application of thermally induced load had a detrimental effect on the fatigue life of the bolted joint. However, compared in terms of the maximum applied resultant bearing stress, $\sigma_{res,max}^b$, biaxial loading is more favourable than the uniaxial loading. Consequently, using uniaxial data for dimensioning of the biaxially loaded joints, in terms of the maximum resultant bearing stress, leads to a conservative design.

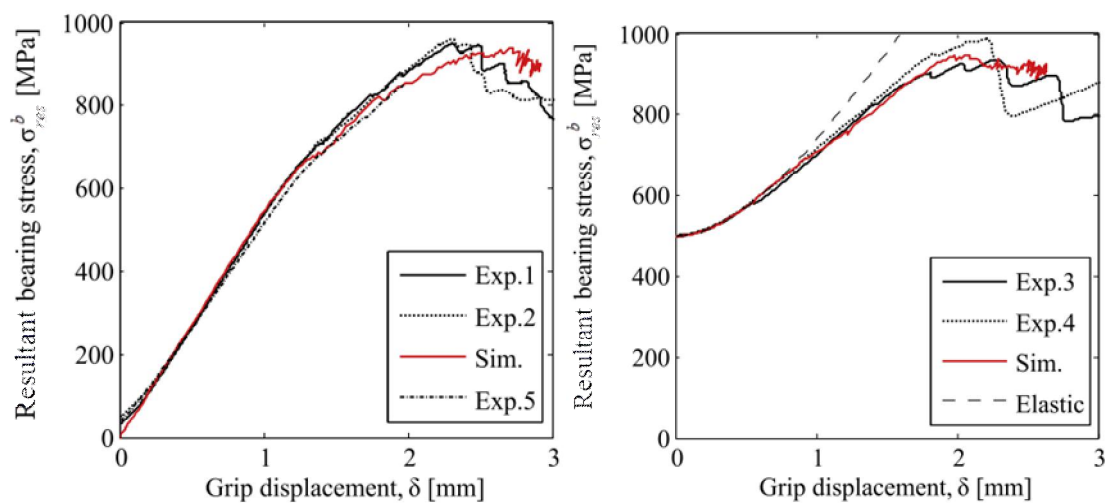


Figure 2. Static bearing failure from experiments (Exp.) and from simulations (Sim.), in uniaxial loading (left) and biaxial loading (right)

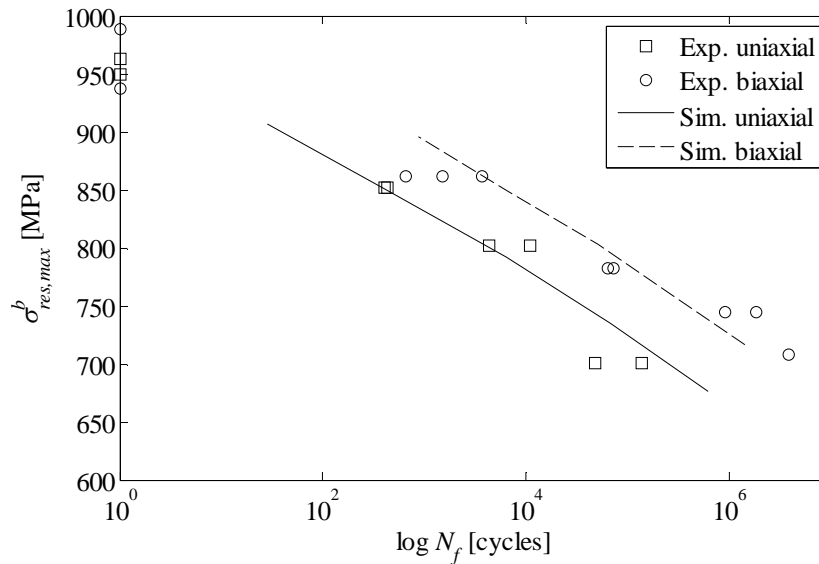


Figure 3. Experimental results (Exp.) from uniaxial and biaxial fatigue bearing tests compared to the simulation results (Sim.) in terms of maximum resultant bearing stress and number of cycles to failure.

- [1] Kapidžić, Z., Ansell, H., Schön, J. and Simonsson, K. (2015). *Compos. Struct.*, vol. 125, pp. 60-71.
- [2] Kapidžić, Z., Ansell, H., Schön, J. and Simonsson, K. (2015). *Compos. Struct.*, vol. 127, pp. 298-307.

3.2 Numerical and experimental study of buckling and collapse of hybrid and integral composite panels - POSCOS

Rolf Jarlås, Joakin Schön, Per Davidsson, FOI

Method development regarding strength prediction and sizing-methods for buckling-critical composite structures has been the theme for the joint FOI-SAAB project called POSCOS. The structures studied are compressively loaded integrally stiffened flat or curved composite panels. Test results are reported for an integrally stiffened slightly curved composite panel and for a panel where aluminium-stringers were bolted to a flat composite skin. Both panels were loaded in compression. The panels were produced by SAAB AB, and the testing was performed at FOI. The test-results contain load-, strain- and full-field measurements using the optical system Aramis. The measurements show that the collapse load is approximately 2.5-3 times higher than the buckling load for the skin. It is also found that applying a limited number of load-cycles well above the buckling load do not cause any observable damage or measurable residual strain. An available analytical method for collapse prediction is discussed and a FE-based method for sizing is presented, together with design charts based on geometrically non-linear finite element analysis. The FE-analysis indicate that the forces between skin and stiffener should be considered as they increase drastically when buckling occur.

Hybrid aluminium-composite panel

A hybrid aluminum-composite structure has been tested in compression to failure to study the effect of buckling [1], figure 1.

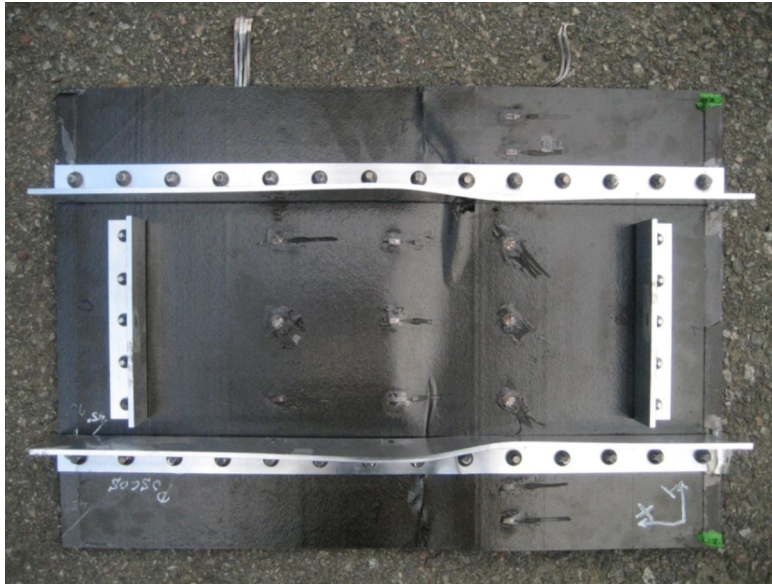


Figure 1. Filed test object with stringers in aluminium

The buckling displacement shape was registered with optical technique (ARAMIS), figure 2. A total of 62 strain-gauges were used to record detailed strains in the specimen. Failure occurred in the measurement area.

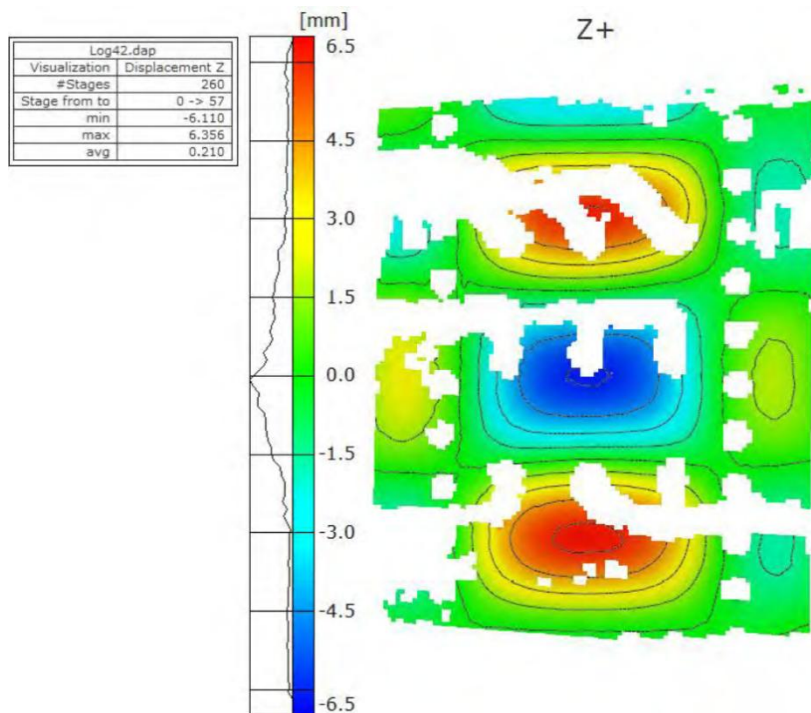


Figure 2. Out-of-plane displacements 490 kN compression load.

Strain reversal was observed at 117 kN and the panel has been loaded to successively higher loads 14 times before the first indication of possible damage occurred at a load being more than three times higher, figure 3. It seems that a single loading to 354 kN, which is three

times above the load at strain reversal (buckling), can be applied without any registration of damage or permanent deformation.

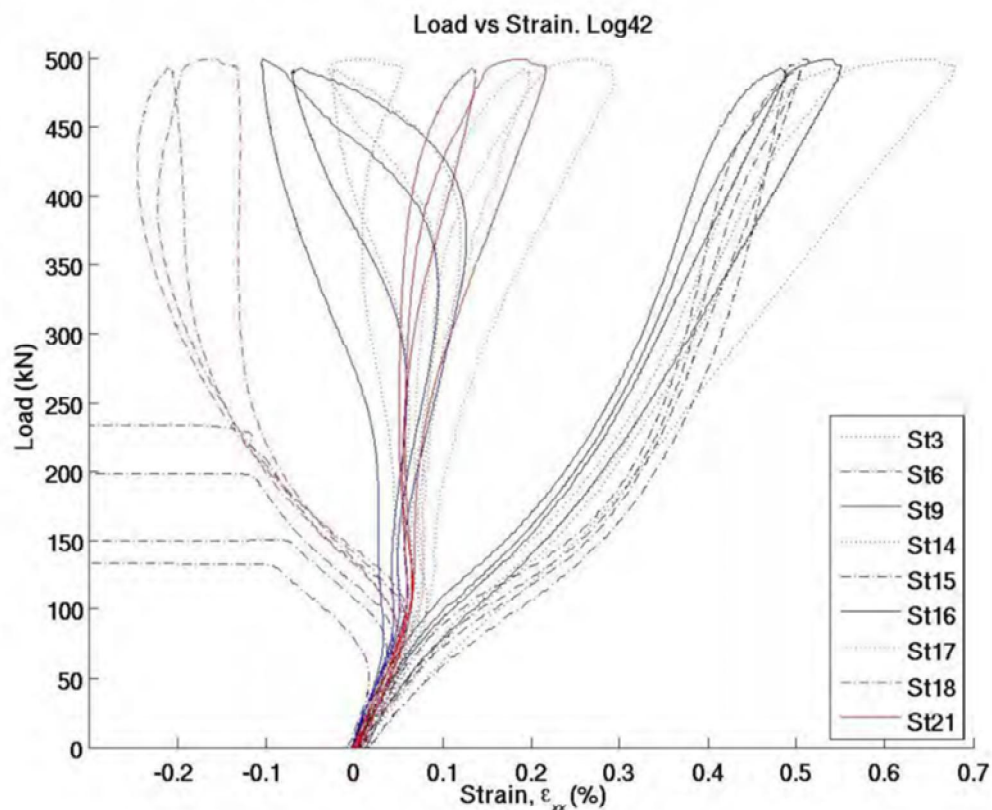


Figure 3. Strain in the loading direction for gauges on the stringer-free side of the skin.

The collapse at 495 kN was very sudden after reaching 499 kN in the previous load cycle with some acoustic noise being heard indicating damage growth. A significantly lower residual strength was indicated by the rapid load reduction, with no intermediate readings of strains between the maximum load and 300 kN. Visual inspection of the panel revealed damage across the skin from one side to the other.

It should perhaps be remarked that by design there is a central part of the panel between the stringers that is prone to buckling and a surrounding region with the stiffeners which is fairly well supported by the test-rig. This panel design with the boundary conditions applied can as shown give very high collapse loads. Conditions where the stiffeners are less supported can be expected to show a lower ratio between collapse load and buckling load.

The test has shown that the load-carrying capacity of the panel is significantly higher than the buckling load for the skin. It has also been shown that a few load-cycles with maximum amplitudes much higher than the buckling load can be applied without causing damage to the panel.

Integral stiffened composite panel

An integral composite structure has been tested in compression to failure to study the effect of buckling [2], figure 4.



Figure 4. Integral composite panel after testing

The buckling displacement shape was registered with optical technique and evaluated with the ARAMIS-system. A total of 62 strain gauges were used to record detail strains in the specimen. C-scan and A-scan were used for post-mortem examination, as there was no visible damage to the specimen after the final load-cycle, although significant residual strains were measured. The scans were however not conclusive, as the dominating echoes are likely to be caused by an adhesive layer introduced during manufacturing of the panel.

Strain reversal was observed at 195 kN and the panel has been loaded to successively higher loads nine (9) times before the first indication of possible damage occurred at a load being about 2.5 times higher. A drastic mode-switch occurred at 375-380 kN, figures 5, 6 and 7, and the panel was loaded five times to higher loads before damage was indicated. The collapse at 522 kN was spectacular and very sudden, but the panel showed a surprisingly high residual strength. The panel was finally loaded to 413 kN before a clear reduction in axial stiffness was observed, and the test was terminated.

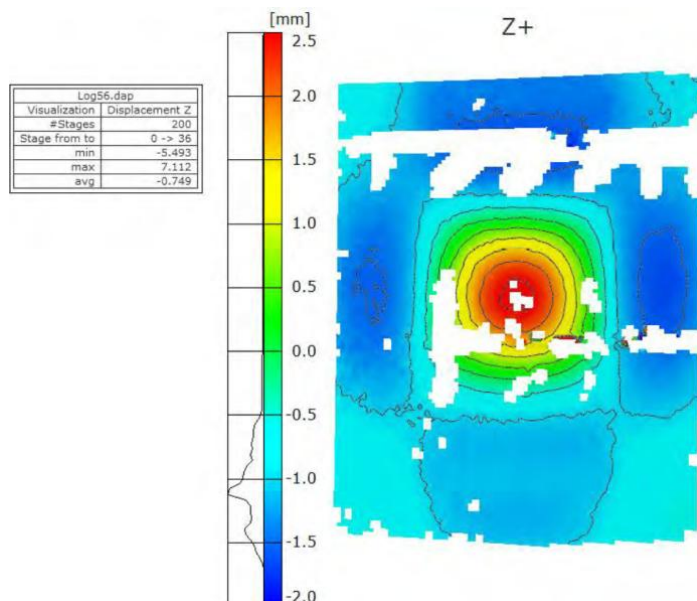


Figure 5. Out-of-plane displacements at 331 kN

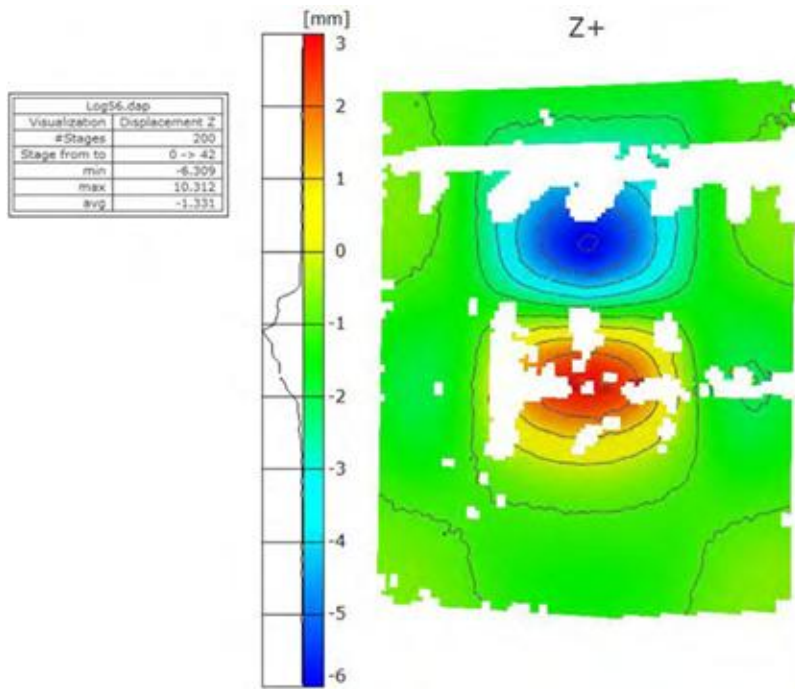


Figure 6. Out-of-plane displacements at 395 kN

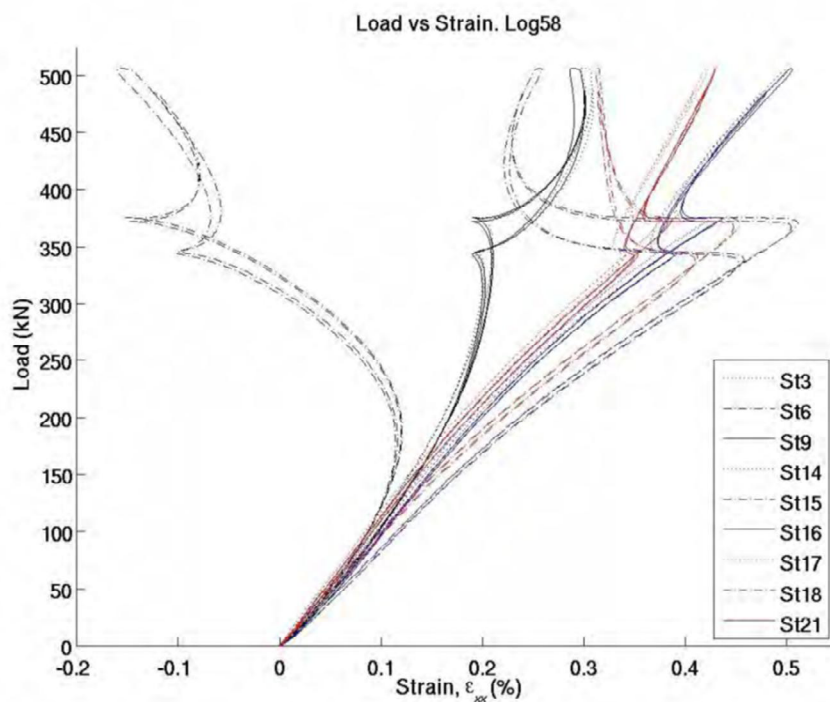


Figure 7. Strain for gauges on the smooth side of the skin

It should be noted that in the test condition there is a central part of the panel that is prone to buckling and a surrounding region with the stiffeners which is fairly well supported by the test-rig. This design can as shown give very high collapse loads. Conditions where the stiffeners are less supported can be expected to show a lower ratio between collapse load and buckling load.

The test has shown that the load-carrying capacity of the panel is significantly higher than the buckling load. It has also been shown that a few load-cycles with maximum amplitudes much higher than the buckling load can be applied without causing damage to the panel.

Analysis and development of a sizing method

Method development regarding strength prediction and sizing-methods for buckling-critical composite structures has been the theme for the joint FOI-SAAB project called POSCOS. The structures studied are compressively loaded integrally stiffened flat or curved composite panels. An available analytical method for collapse prediction is discussed and a FE-based method for sizing is presented, together with design charts based on geometrically non-linear finite element analysis [3]. The FE-analysis indicate that the forces between skin and stiffener should be considered as they increase drastically when buckling

- [1] Jarlås R., Schön J., Davidsson P. ,Test of integral composite panel loaded in compression. FOI-R-3844--SE, 2014
- [2] Jarlås R., Schön J., Davidsson P. ,Test of hybrid panel loaded in compression. FOI-R-3843--SE, 2014
- [3] Jarlås R., Sizing of composite panel loaded in compression. FOI-R-3842--SE, 2014

3.3 Development and implementation of a method for in-service interpretation and decision regarding temporary acceptance of damage in composite structure

Christina Altkvist, Michael Ringquist, Saab AB

Introduction

The maintenance documentation for the Gripen Fighter Aircraft consists of a number of publications needed to maintain and repair the aircraft throughout its life cycle. Two of these are the Aircraft Maintenance Publication (AMP) and the Aircraft Repair Publication (ARP). The intention of AMP is primarily to provide the required instructions and directives for maintenance of the Gripen weapon system and the intention of ARP to form the basis for the repair work on the aircraft.

The ARP contains mainly instructions for permanent repair of different zones of the aircraft. However there is also a need for temporary repair procedures that restore the load-carrying capability of the structure for a limited period of time allowing the operator to use the aircraft optionally under maneuver restrictions until permanent repair can be carried out. For this purpose a concept for a new publication RTRP (Restrictions and Temporary Repair Publication) has been developed. The purpose of RTRP is to give the operator documentation for the assessment and classification of damages and to identify associated restrictions on flight operations.

The RTRP concept consists of

- Procedures for damage detection including NDT methodology with lower requirement on educational level for the operator
- Procedures for damage assessment and classification of damages
- Associated restrictions for operation of the aircraft with classified damages
- Simple repair methods

The concept has been tested on structural parts subjected to frequent damages. One of this is the Gripen canard composite skin which has been analyzed in the following way.

Damage categorization

The various types of damages that might occur in the canard skin structure have been divided into three categories of damages – surface damages, in- depth damages and edge damages. Within each category different types of damages can be found such as scratches, heat impact, dis-bonding etc.

Damage detection

Damages in aircraft structures are normally detected during maintenance or turnaround. If a visual inspection reveals damages the inspector in most cases request a NDT/NDI to determine the extent of the damage. Inspections on composite structures require qualified personnel in non-destructive testing (NDT) with specialist knowledge in composite testing. With this new approach it is possible for an operator with lower requirement on education level (referred to as Level 1 limited) to carry out an NDT inspection with the Pitch Catch method. The intention is to get an idea of the size of the potential damage and with this method damages with a minimum size of 25 x 25 mm can be detected.

The upper and lower skin of the canard is divided into different zones and in each zone acceptable damages with no restrictions and with maneuver restrictions for a limited period of time are specified.

The RTRP concept has been verified by letting maintenance technicians at the wings practice the concept. For this purpose a reference laminate with different types of hidden and visible damages was manufactured and used together with the pitch catch equipment and applicable publications (AMP, ARP and RTRP).

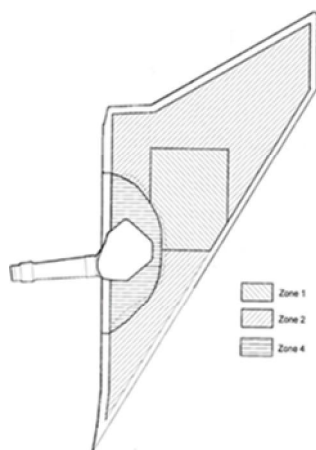


Figure 1. Canard wing lower skin, zone sections Figure 2. Testing of Pitch Catch equipment

Damage size definition

From a stress point of view the assessment of an existing damage in the composite skin panel will be interpreted as an existing hole in the structure. This is in general a conservative interpretation of the damage. Depending of the size of the damage, five damage size categories have been specified;

Size category	Damage size D_{hole} (mm)
1	$0 < D \leq 6$
2	$6 < D \leq 25$
3	$25 < D \leq 50$
4	$50 < D \leq 75$
5	$75 < D$

All existing damages in the Canard upper and lower skin has to be assessed in accordance with these damage size categories which mean that any damage e.g. a scratch or a delaminated area discovered by NDT shall be defined by a circular circumference covering the whole damage and measured by diameter.

Acceptable strain level related to damage size

The relation between an existing damage in the composite skin and the level of strain that can act in this structure without any risk of structural failure is developed and established by analysis and test results.

Specific assumptions are made in the establishment of allowable strain, e.g. tension and compression are treated in the same way, both hole and impact damage are covered by the allowable value.

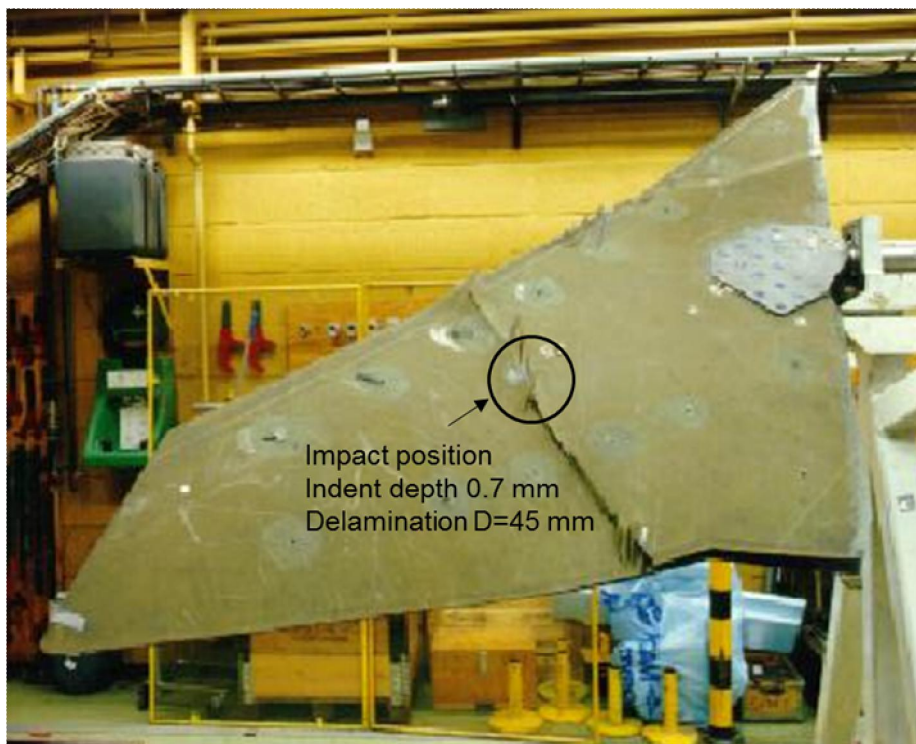


Figure 3. Verification test to failure of an impact damaged canard wing.

Relation between strain level and load condition

The specific structure must be analyzed regarding relation between acting load condition and the related strain levels that act in the skin. A variety of load conditions is generated with different levels of load factor, speed and altitude. Acting strain in a specific area of the skin is analyzed for all these load conditions. This enables to create a connection between the maneuver envelope extension and adherent strain levels acting in the skin.

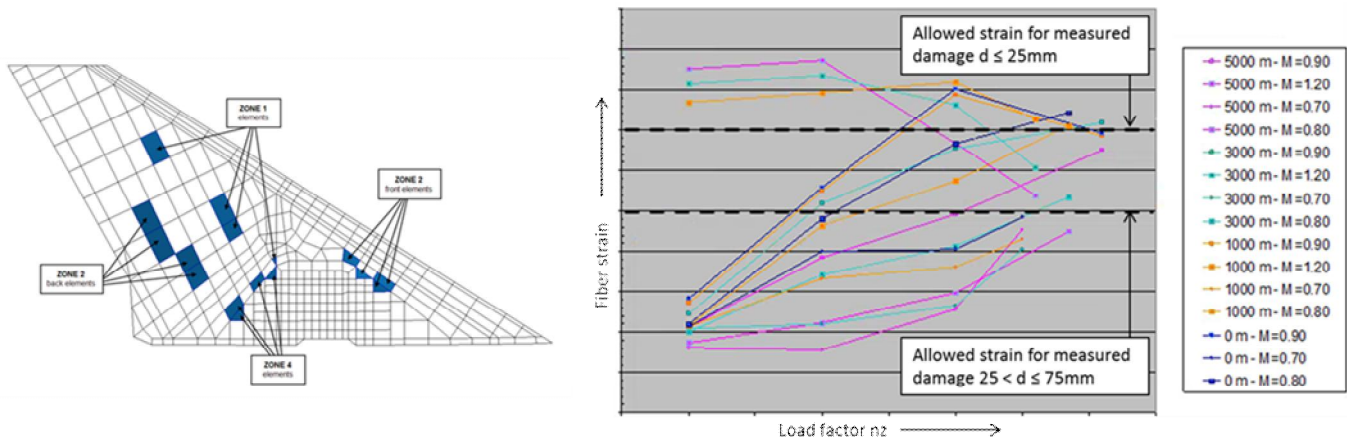


Figure 4. Fiber strain levels in specific area under different maneuvers

Operating the aircraft under any restricted level is strictly connected to a limited period of 50 flight hours or six months depending on which comes first. The structural damage shall thereafter be repaired for restoration of the strength to ensure that the durability is not affected.

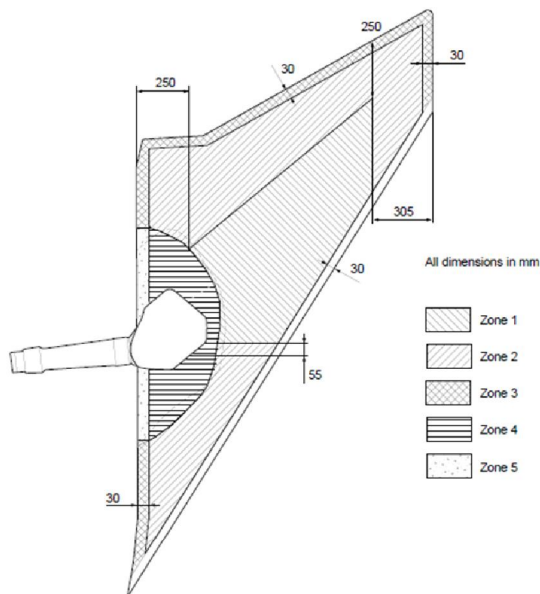


Table 17 Top skin, repair procedures (approval level I)

Zone	Permitted damage	Damage type	Repair procedure
1, 2	$d < 6$ mm	Surface damage, damage at depth	4.2.101, 4.2.102. Refer to the ARP J3-A-00-17-42-01A-600A-A.
2	$d < 75$ mm	Surface damage	4.2.101. Refer to the ARP J3-A-00-17-42-01A-600A-A.
3	$L < 40$ mm, $W < 10$ mm	Edge damage	4.2.113, 4.2.114. Refer to the ARP J3-A-00-17-42-01A-600A-A.

Effectivity: 39C, D J3-A-31-30-00-01A-660A-A

Table 17 Top skin, repair procedures (approval level I) (Continued)

Zone	Permitted damage	Damage type	Repair procedure
4	$d < 50$ mm	Damage at depth	4.2.115. Refer to the ARP J3-A-00-17-42-01A-600A-A.
	Damage below the Rohacell layer cannot be repaired		
	Alternative:		
	Change all or a part of the Rohacell core. Part number 1903211-541		
5	$L < 100$ mm, $W < 20$ mm	Edge damage	4.2.116. Refer to the ARP J3-A-00-17-42-01A-600A-A.
	Damage below the Rohacell layer cannot be repaired		

Figure 5. Example of ordinary repair procedure: Upper skin of canard wing

3.4 Analysis and testing of a linerless demonstrator tube at cryogenic temperatures and made of thin carbon plies

Mats Dalenbring, Per Davidsson, Joakim Schön, FOI

An EU-funded study called CHATT (Cryogenic Hypersonic Advanced Tank Technologies) was initiated 2012. The project CHATT is part of the European Commission's Seventh Framework Programme and run on behalf of the Commission by DLR-SART in a multinational collaboration. One of the core objectives is to investigate Carbon Fiber Reinforced Plastic (CFRP) cryogenic pressure tanks.

The main objective was to find good laminate design candidates for experimental testing and possible future production [1]. One focus is on tank design without liners. A challenging task is to avoid leakage of the tank at prescribed loading conditions. The approach taken here is to use very thin plies and many layers. The most promising tank designs will be tested.

Analysis

A detailed ply resolved numerical FE model of the tank laminate specimen was built. In this context, inter laminar stresses resulting from loading and miss-match in thermal expansion coefficients due to material anisotropy may thus be resolved and evaluated. For this purpose, the model will be based on the use of the FOI in-house higher-order FE code Stripe. In the present study a detailed ply resolved numerical 3-dimensional volume FE model of the tank laminate specimen is set-up. The FE model was mapped onto the exact cylinder geometry. This model was verified from basic simulations using only a thermal load.

Finally, optimal laminate stacking sequences that will introduce a low amount of thermal stress and damage was evaluated. The optimization was done using a FOI in-house Matlab® based tool. Two types of optimization were chosen. The first one is based on differential evolution (DE) algorithm and the second is based on so-called pattern search. The two search algorithms are demonstrated on the classical Matlab® surface. In the tank optimizations only the DE algorithm were used.

The design parameters used are the 20 fibre angles in a symmetric 40 layer laminate. The stresses are calculated in Stripe followed by cost function/merit value evaluation in Matlab® and generation of new search. A suitable design evaluation criteria with respect to stress, damage and leakage for the optimization, was chosen based on the idea that it is favourable to have a region in the laminate with a low level of stress in the matrix. The measure used in the optimization is that stresses perpendicular to the fibre direction should be minimized. Finally, an unconstrained optimization was performed on the tank. The trivial result with all fibre angles oriented in the same direction, introducing the least amount of thermal miss-match, was found by the optimizer.

A constrained optimization is therefore necessary in order to find realistic laminate stacking sequences. A first constrained optimization using a thermal load has been performed. The obtained stacking sequence is shown in figure 1 and it is quite different from an ordinary stacking sequence. This solution was then adjusted (green curve) to decrease the number of fibre angles and to have at least 10 degrees difference in fibre angle between two different layers. The effect on the stress level is minor.

Finally, an optimisation with thermal- and mechanical loading was performed to mimic the experimental leakage tank test performed at FOI. The final result from the constrained optimization, using a combined thermal and mechanical loading, shows that the optimizer was not able to come up with a stacking sequence better than the $\pm 25^\circ$ tank that was proposed by SICOMP and successfully tested for leakage at FOI in WP 3.6. In fact, after 80 DE iterations using a population of 200 individuals, resulting in 16 000 finite element calculations, the $\pm 25^\circ$ tank is still 40% better. Of course our problem could have been reduced further into a one-dimensional problem considering only "one" angle but the purpose was here to set-up and use a more general setting in the optimization tool. This result suggests that external applied loads dominate over internal thermal stresses.

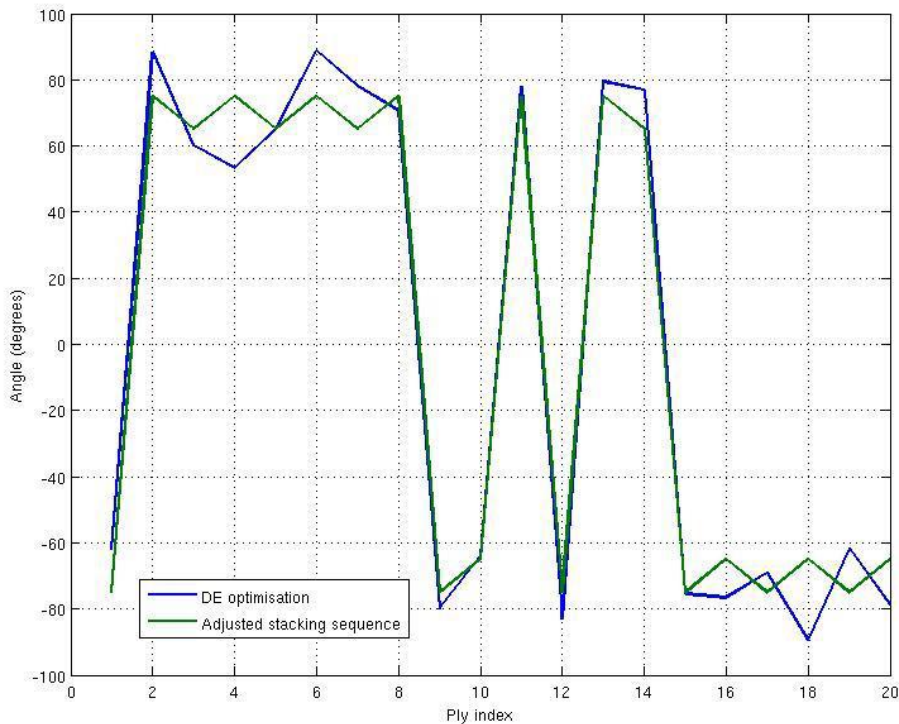


Figure 1. Best and adjusted stacking sequence.

Testing

A linerless tank concept has been tested at cryogenic temperatures in the form of a linerless demonstrator tube made of thin carbon plies [2]. From the obvious similarity between the force and strain curves in the loading experiment (Figure 1) it can be concluded that the irregularities e.g. between 205 s and 243 s are due to relaxation elsewhere in the load chain. This should therefore not influence the actual leak measurement. The slow increase in helium flow basically following the strain indicates the presence of minor initial matrix cracks slowly widening as load and strain increases. The similar behaviour of the health monitoring voltage may be explained either by a slight misalignment of the voltage taps or an asymmetric anisotropy about the length axis making the carbon fibre reinforcement acting as a strain gauge itself.

At second 346 there is a sharp change in the monitoring voltage (approx. 3 μV) which after 3 seconds is followed by a clear increase in helium flow. This is fully consistent with the expected response time of the leak detector arrangement. The second leak increase at 362 s cannot clearly be predicted in the monitoring signal indicating that another failure developed away from the area covered by the monitoring bridge even though it was followed by a sharp increase in pressure in the vacuum jacket and an immediate saturation and down-throttling of the leak detector sensitivity. The third occurrence, the dramatic change in monitoring voltage at 368 s is probably caused by a propagation of the first failure even if it could not be recorded in the leak signal. After 383 s one can see an onset of dissimilarity between force and strain as an indication of progressing structural damage. After 394 seconds the experiment was manually aborted to avoid further damage.

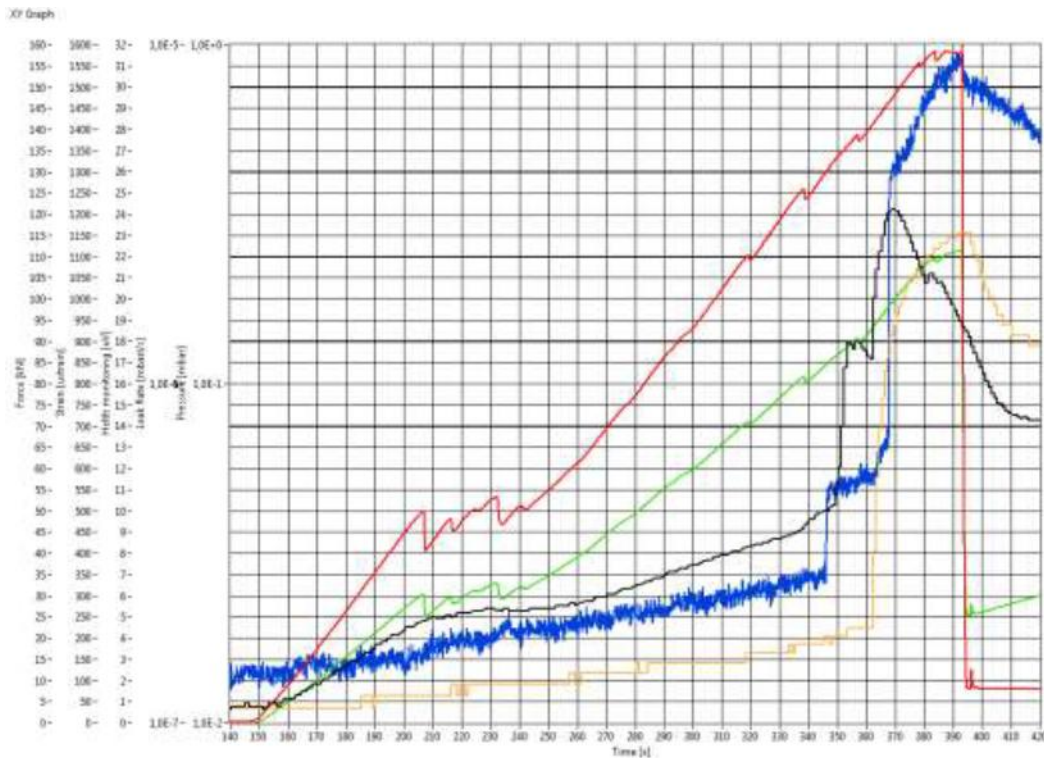


Figure 1. Diagrams showing the development of applied force (red), strain in the cold region (green), output from the health monitoring bridge (blue), He leak rate (black, logarithmic scale) and pressure in the vacuum jacket (orange, logarithmic scale) for the entire load increase and for a portion around the onset of failures.

- [1] Mats Dalenbring, Report on stress and damage optimization computations for the WP3.4 demonstrator, Deliverable D3.4.1, EU-project CHATT Cryogenic Hypersonic Advanced Tank Technologies, (2015).
- [2] M. Loukil, K. Olofsson, and P. Davidsson, Design, manufacturing and testing of linerless demonstrator tanks, Deliverable D3.4.5 and D3.6.1 Report on testing of tubes and results from material screening, EU-project CHATT Cryogenic hypersonic advanced tank technologies, (2015)

4 THERMAL MECHANICAL FATIGUE OF SUPERALLOYS

4.1 Dwell time crack growth at high temperature in a Ni-based superalloy

Erik Storgårds, LiU

In high temperature applications, e.g. gas turbines, crack growth have been seen to not only be affected by cyclic load but also from dwell times, e.g. sustained load. To meet new design criteria and extend life of current components a research project, at Linköping University, within the research programme TURBO POWER was initiated, see [1]. The programme has been running for 2 phases, the first from 2007-2011 followed by a second phase, 2012-2015, led by the Swedish Energy Agency, GKN Aerospace Engine Systems and Siemens Industrial Turbomachinery AB. The second phase of the programme has focused on increasing the Technological Readiness Level (TRL) for dwell time models, which can increase both reliability and safety for gas turbine manufacturers.

Initially, testing has been performed on Inconel 718 (commonly used in engine applications), with emphasis on surface cracks subjected to dwell times and a mix on dwell times and cyclic load, see e.g. [2]. Subsequent modelling work has concentrated on creating a model that is reliable to use, easy to calibrate parameters for and require low amount of computational recourses. As a result, the modelling work has taken a phenomenological approach with physically motivated parameters, describing dwell damage by what is seen in fracture paths. Analyses of crack paths have shown that dwell times induces grain boundary damage, in contrast to cyclic load where mainly transgranular cracking is observed. As a result, this damage behaviour has been incorporated by describing dwell damage and cyclic load by these 2 different crack growth modes. By following the load modes in what order they are applied a history dependent model is also achieved, which substantially increases the accuracy compared to traditional models (who separately applies each growth mode).

A number of different studies have been conducted within the project to prove the concept of the model and extend it for the conditions seen in gas turbines, as well as increase the understanding of dwell time crack growth. These include analysis of engine spectra loadings, overloads in combination with dwell times and thermo-mechanical fatigue crack growth at stress concentrations, all at high temperature. As an example to show on the capabilities of the model, a relevant engine spectrum has been tested and simulated at 550°C, see below.

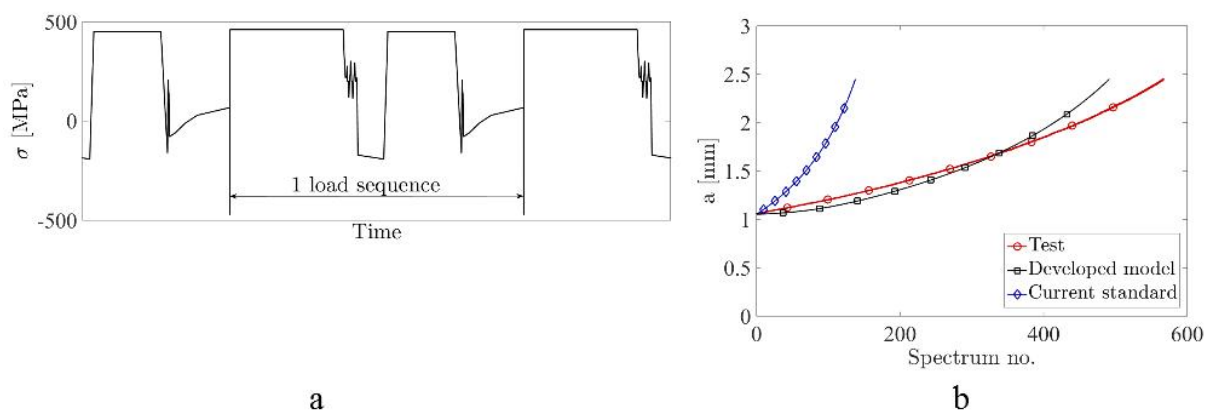


Figure 1. (a) Engine spectra with dwell times and (b) simulation results, both for the developed model and current industry standard From [3]

- [1] <http://www.turbokraft.se>.
- [2] E. Lundström, K. Simonsson, D. Gustafsson, and T. Månsson, A load history dependent model for fatigue crack propagation in Inconel 718 under hold time conditions. *Engineering Fracture Mechanics*, 118:17 – 30, 2014
- [3] E. Lundström, K. Simonsson, T. Månsson, and D. Gustafsson, Modelling of fatigue crack growth in Inconel 718 under hold time conditions - application to a flight spectrum *Advanced Materials Research*, 891-892:759–764, 2014

4.2 Test facility for Thermal Mechanical Fatigue – TMF

Per Sandahl, Exova Technology AB

Turbine blades in aircraft engines are subjected to a variety of stresses. In operation, the mechanical load is large, the blades are in a corrosive environment with exhaust gases and fuel and they are also exposed to high temperatures.

To obtain fatigue data for the material, strain-controlled fatigue testing is used, low cycle fatigue (LCF). LCF testing is used at a constant temperature. LCF testing is an approximate comparison with reality when temperatures are rarely constant for the materials, example when a turbine engine starts the temperature is low. When the engine is getting hotter the stress also increases. To simulate start, stop, and running of an engine, a new test method have been developed, thermal mechanical fatigue testing, TMF. TMF testing is just like the LCF test strain-controlled. The difference is that the temperature varies during the strain cycle.

Siemens Industrial Turbinmachinery Sweden has worked with TMF testing for over 15 years. In 2007 Exova Materials Technology AB was asked to invest in a TMF equipment and start testing for Siemens. This has been done successfully and the facility has recently been extended with a third test rig.

The current capacity of the test facility is:

- 100 kN load cell
- 50-1000 °C at 10 °C/s
- A digital image system for crack length recording



Figure 1. TMF test rig at Exova Technology, Sweden

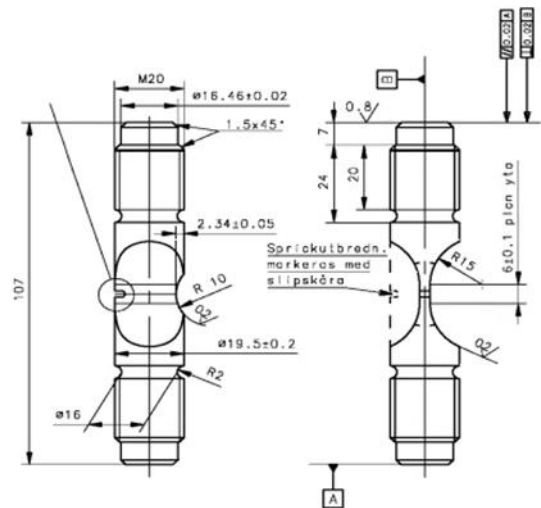
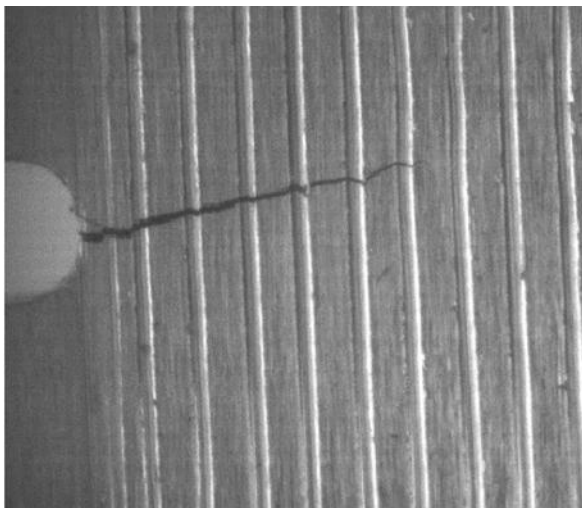


Figure 2. Digital image recording system for crack length measurement

4.3 Mechanical behaviour and microstructure in selective laser melted Hastelloy X

*Håkan Brodin, Olov Andersson, Siemens
Sten Johansson, LiU*

Selective laser melting (SLM), or, as the industry standard denotes the process, laser sintering, is an additive manufacturing process where metal powder is melted by a laser source layer-wise, forming a solid, dense metallic component. With the SLM process, near net shape components can be manufactured directly from a CAD model. The model is sliced into thin (max 100 μ m thick) layers. Powder is distributed onto a metallic build platform and the powder is fused by a laser as dictated by the CAD model. The laser energy is intense

enough to permit full melting (welding) of the particles to form solid metal. The process is repeated layer by layer until the part is complete.

A number of materials are available, including steel, aluminium, titanium and, in recent time, also superalloys. The material investigated in the current project is an alloy in agreement with the composition of Haynes International Hastelloy X, a solution strengthened superalloy typically used in large welded components exposed to high temperatures in oxidizing as well as reducing environments.

Microstructurally, the material is different from both a hot-rolled, as well as a cast material due to the manufacturing process. Since the SLM process involves laser melting of powder particles in the size range of $<50\mu\text{m}$, the structure resembles of a weld structure, however on a smaller scale. Due to the layer-by-layer build strategy, the material will exhibit anisotropy. Different heat treatment approaches can be adopted in order to homogenize the material and to minimize the effect of anisotropy.

The current project focuses on evaluating mechanical properties for a material manufactured by the SLM process and comparing to data for established manufacturing processes. For evaluation of the mechanical properties, low cycle fatigue testing and tensile testing has been performed. The microstructure and material deformation / cracking are evaluated by light optical microscopy and SEM, where electron backscatter diffraction is used. Due to the weld-like structure, the material will be transversely isotropic in the as-manufactured condition with one symmetry plane perpendicular to the build direction. Any direction perpendicular to the build direction tends to give increased strength compared to a direction parallel to the build direction if monotonic data are concerned. If fatigue properties are concerned, the anisotropy is also obvious. It is shown that the differences in behaviour can be coupled to microstructure.

The current work is performed on material produced with selective laser melting (SLM) and evaluated by light optical microscopy, scanning electron microscopy and mechanical testing. Results are obtained from tensile testing, low cycle fatigue, thermomechanical fatigue and creep testing together with microstructural evaluation with light optical microscopy and scanning electron microscopy.

Results and discussion

Findings in mechanical testing indicate that the material is highly anisotropic regarding the tensile properties (yield stress and ultimate tensile stress). Compared to a hot-rolled material, the material yield strength is considerably higher in the 0° direction, at least a factor of 2 up to 700°C . Even at higher temperature, the material data fall well above the average data of a hot-rolled material.

Upon comparison, the yield strength of the material decreases when the build angle α increases. This is visualized below, where different loading directions are compared to the hot-rolled material at 400°C , figure 1.

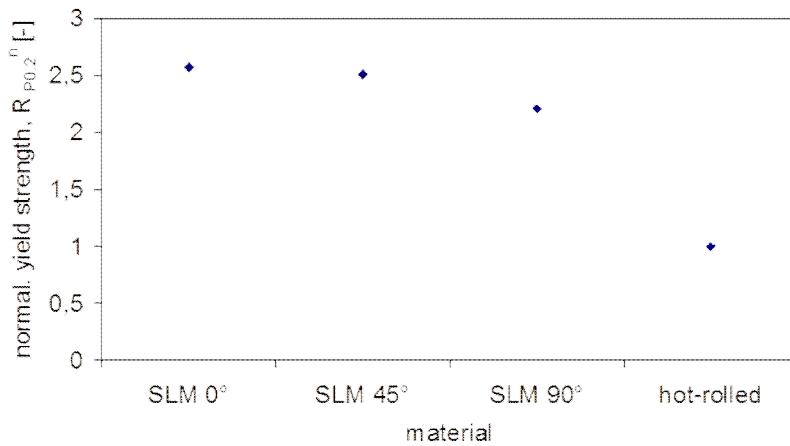


Figure 1. Normalized yield stress for the three SLM directions compared to hot-rolled material. Test temperature 400°C.

From an LCF perspective, the data show a slightly different picture. The direction that gives the longest fatigue life is the 90° direction. Fatigue life data in the 90° direction are comparable to hot-rolled materials. Loading in the 0° and the 45° directions does not give a conclusive picture, but there is a tendency to a slightly longer life if the material is loaded in the 0° direction compared to the 45° direction. A comparison between the different materials is given below, Figure 2.

Comparing the mechanical testing to microstructural findings confirms that the material is anisotropic. The material is clearly anisotropic due to the weld-like structure. When comparing to the EBSD data and pictures of heat treated material, it is even more obvious that the material is anisotropic. The photos reveal that the grain structure observed is columnar with grains elongated along the build direction and a small diameter in the build plane. From this aspect it seems logical that the yield stress is highest in the direction with the smallest observed grain size due to a grain size strengthening effect.

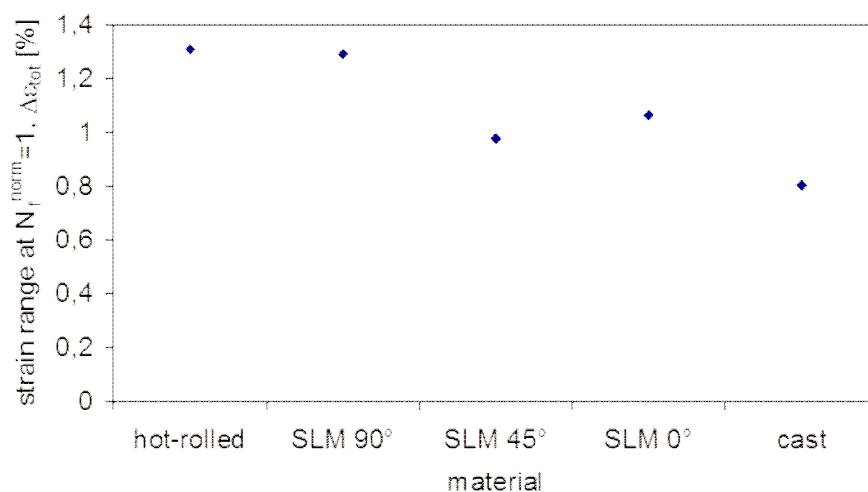


Figure 2. Strain range to failure for the different loading directions at normalized fatigue life $N_{f, norm} = 1$.

TMF and creep results for SLM Hastelloy X clearly show that the high temperature mechanical behaviour of the SLM material is inferior to a material manufactured by

traditional manufacturing routes. A major difference between SLM material and hot-rolled or cast materials is the grain size that is significantly smaller in the SLM material. The microstructures shown above indicate that the SLM material has a grain size that is dependent on direction. This is reflected in the material data, where the 0° direction exhibits poor creep behaviour. In this direction, the material behaves as a very fine-grained material. When the loading direction is altered towards the 90° direction, the creep resistance is improved and the material behaves more like a coarse-grained material manufactured by a traditional manufacturing method. One explanation why fatigue resistance is lowered in the TMF tests is creep-fatigue interactions, where the 300s dwell time at maximum temperature allows for creep to take place in every TMF cycle. Hence, the direction that will behave poorly in TMF, well corresponds to the direction that is inferior in creep behaviour. Furthermore, the material is not heat treated in the same way as a hot-rolled or cast material. The material does not contain carbides to the same extent as a cast or hot-rolled material. Therefore the creep and high temperature fatigue resistance is likely to be reduced.

Conclusions

From the findings in the current work it can be concluded that the SLM material is anisotropic in the as manufactured condition from a microstructural as well as from strength and fatigue aspects.

Microstructurally, the material is considered to have a weld structure with grains elongated in the build direction. The grains extend over several weld pass layers in the material. In the light optical micrographs it is observed that the material has a needle-like structure. After heat treatment at 900°C, the needle-like structure disappears and, instead, carbides are found at the grain boundaries.

Tensile properties are superior to standard hot-rolled material in all investigated directions 0°, 45° and 90°. The microstructure is very fine-grained and fine grains will contribute to the strength of the material.

Fatigue tests indicate that the material has the highest resistance against fatigue crack growth if built and loaded in a direction parallel to the build direction. It is also shown that the crack growth direction is influenced by the SLM build direction.

A heat treatment is needed in order to remove the weld structure and to reduce the anisotropy.

[1] Brodin H, Andersson O, Johansson S, Mechanical testing of a selective laser melted superalloy, 13th international conference on fracture, June 16-21, 2013, Beijing, China

[2] Brodin H, Andersson O, Johansson S, Mechanical behaviour and microstructure correlation in a selective laser melted superalloy, ASME Turbo Expo 2013, Turbine Technical Conference and Exhibition, San Antonio, TX, June 3-7, 2013

ACKNOWLEDGEMENTS

This editorial work was supported by Saab AB. The editor is also indebted to the following individuals who helped to write this review:

Zlatan Kapidzic	Saab AB	(Section: 2.1, 2.3, 3.1)
Christina Altkvist	Saab AB	(Section: 3.3)
Michael Ringquist	Saab AB	(Section: 3.3)
Magnus Kahlin	Saab AB	(Section: 2.2, 2.4)
Joakim Schön	FOI	(Section: 3.1, 3.2, 3.4)
Rolf Jarlås	FOI	(Section: 3.2)
Erik Storgårds	LIU	(Section: 4.1)
Per Sandahl	Exova	(Section: 4.2)
Håkan Brodin	Siemens	(Section: 4.3)